Supplemental Material: Observation of Chemical Reactions between a Trapped Ion and Ultracold Feshbach Dimers

H. Hirzler,[1] R. S. Lous,[1] E. Trimby,[1] J. Perez-Ríos,[2,3,4] A. Safavi-Naini,[5,6] and R. Gerritsma[1,5]

[1] *Van der Waals-Zeeman Institute, Institute of Physics, University of Amsterdam, 1098 XH Amsterdam, Netherlands*
[2] *Fritz-Haber-Institut der Max-Planck-Gesellschaft, Faradayweg 4-6, 14195 Berlin, Germany*
[3] *Institute for Molecules and Materials, Radboud University, Heyendaalseweg 135, 6525 AJ Nijmegen, Netherlands*
[4] *Department of Physics and Astronomy, Stony Brook University, Stony Brook, New York 11794, USA*
[5] *QuSoft, Science Park 123, 1098 XG Amsterdam, the Netherlands*
[6] *Institute for Theoretical Physics, Institute of Physics, University of Amsterdam, Science Park 904, 1098 XH Amsterdam, the Netherlands*

(Dated: March 14, 2022)

ION TRAPPING FREQUENCY CALIBRATION

We measure resonant heating of various Yb^+ isotopes to calibrate the trapping frequency of our Paul trap. The ion's radial trap frequency in the x-direction can be expressed by [1]

$$f_m \equiv \omega_x/2\pi \approx \sqrt{\left(\frac{-k_x Q U_{dc}}{m y_0^2} + \frac{{k'_x}^2 Q^2 U_{rf}^2}{2m^2 r_0^4 \Omega^2}\right)} \quad (1)$$

$$\equiv \sqrt{\frac{\kappa_x}{m} + \frac{\kappa'_x}{m^2}}, \quad (2)$$

with Q the electric charge of an ion with mass m, trap parameters r_0 and y_0, U_{rf} and U_{dc} the radio-frequency (rf) and direct-current (dc) voltages respectively, and geometrical factors k_x and k'_x. Here, the trap parameters are combined into new factors κ_x and κ'_x. Without atoms, we measure f_m for the isotopes $^{168}Yb^+$, $^{172}Yb^+$, $^{174}Yb^+$ and $^{176}Yb^+$, by resonantly driving the trap frequency with low driving voltage of 0.05 Vpp. Due to the Doppler shift, successful heating is visible by reduced ion fluorescence. The results are presented in Fig. 3 (lower panel) of the main text. We fit Eq. 2 (orange line) to extract κ_x and κ'_x and use these to calculate a theoretical trap frequency for the $^6Li^{174}Yb^+$ molecular ion of $f_{res} \approx 183.4$ kHz (blue dash-dotted line). Note, that we observe day-to-day frequency drifts on the order of 0.5 kHz which we compensate by daily referencing to f_{174}.

OBSERVATION OF DARK IONS

We observe dark ions after the interaction with the neutral cloud. We explain their origin in photodissociation of molecular ions with the 1064 nm ODT light, similar to observations with $BaRb^+$ reported in Ref. [2]. After the interaction with the cloud, we record fluorescence with a photomultiplier tube (pmt) every 50 ms over 1500 ms, whereby the detection time for each data point is 2.5 ms. For each fluorescence measurement, we project the photon count to represent a bright (fluorescent) ion or a dark (non-fluorescent) ion. Then, we combine the photon counts from all measurements into a histogram and we define a threshold between the partially separated peaks for bright and dark ions. Varying the threshold by 20 %, we do not find a significant deviation on our results.

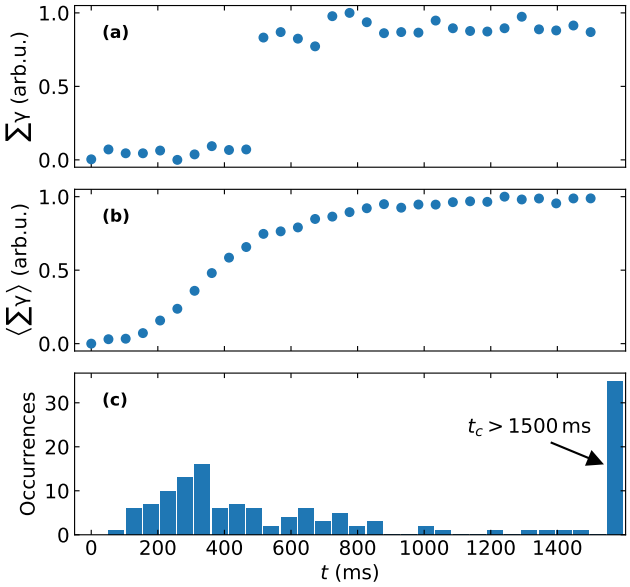

FIG. 1. Photon count ($\Sigma\gamma$) during Doppler cooling after an ion-neutral collision averaged over 2.5 ms detection time. (a) Single-shot photon count for a dark ion. (b) Average photon count and (c) histogram for all dark ions observed in scanning the ODT power in the main text.

For the P_{ODT} scan data (Fig.2) of the main text, Fig 1a) shows a typical single shot photon count for a dark ion turning bright again after about 500 ms of Doppler cooling, together with in b) the fluorescence averaged over the entire data set. The same data is shown as a histogram in c), where the contribution from lost ions ($t_c > 1500$ ms) can be seen.

CREATION OF DIMERS AND DENSITY MODEL

The dimers are created by three-body recombination during evaporation close to the 832 G Feshbach resonance (FR). This particular resonance has been widely studied (e.g. [3, 4]) and we can use the insights from [5, 6] to calculate the dimer density in our system.

Rate Equations

For a positive scattering lengths ($B < 832\,\mathrm{G}$) and a sample initially consisting of atoms, three-body recombination is the dominant process to form dimers,

$$\mathrm{Li} + \mathrm{Li}' + \mathrm{Li} \rightarrow \mathrm{Li}_2 + \mathrm{Li}. \tag{3}$$

The dissociation process is the other way around,

$$\mathrm{Li}_2 + \mathrm{Li} \rightarrow \mathrm{Li} + \mathrm{Li}' + \mathrm{Li}, \tag{4}$$

and the two spinstates of lithium are indicated by Li and Li′. The formation rate coefficient is given by $R_{3r} = 167a^6 k_\mathrm{B}T/\hbar$ when $E_\mathrm{b}/k_\mathrm{B}T \gg 1$ [7], with E_b the binding energy of the dimer. Here, a is the atom scattering length, k_B the Boltzmann constant, T the atom temperature and $\hbar$ Planck's constant h divided by 2π. In the halo-regime where $E_\mathrm{b}/h < E_\mathrm{vdW}/h = 614\,\mathrm{MHz}$, with van der Waals energy E_vdW, this results in $R_{3r} \approx 167\frac{\hbar^5}{m_\mathrm{a}^3}\frac{k_\mathrm{B}T}{E_\mathrm{b}^3}$ and the dissociation rate $C_d = 3.75\frac{\hbar^2}{m_\mathrm{a}^{3/2}}\frac{(k_\mathrm{B}T)^{5/2}}{E_\mathrm{b}^3}e^{-E_\mathrm{b}/(k_\mathrm{B}T)}$ for the reverse process [5]. This leads to the following rate equations

$$\frac{dn_\mathrm{a}}{dt} = -4R_{3r}n_\mathrm{a}^3 + 4C_d n_\mathrm{a} n_\mathrm{d} \tag{5}$$

$$\frac{dn_\mathrm{d}}{dt} = 2R_{3r}n_\mathrm{a}^3 - 2C_d n_\mathrm{d} n_\mathrm{a}. \tag{6}$$

where n_a is the atom density of a single spin state and n_d the dimer density. Here, we assume that all atoms and dimers remain trapped even after colliding and thus that $E_\mathrm{b} \ll U_\mathrm{trap}$, the trap depth which is about $20(14)\,\mu\mathrm{K}$.

Thermal Equilibrium

In thermal equilibrium, $\frac{dn_\mathrm{a}}{dt} = \frac{dn_\mathrm{d}}{dt} = 0$, and assuming the atoms and molecules thermalize ($T = T_\mathrm{a} = T_\mathrm{d}$), Eq. 5 simplifies to an analytic expression

$$n_\mathrm{d} = \frac{R_{3r}}{C_d}n_\mathrm{a}^2 = 2^{3/2}\left(\frac{2\pi\hbar^2}{m_\mathrm{a}k_\mathrm{B}T_\mathrm{a}}\right)^{3/2} n_\mathrm{a}^2\, e^{E_\mathrm{b}/(k_\mathrm{B}T)}. \tag{7}$$

In terms of phase space density, the equation can be rewritten as $\phi_\mathrm{d} = \phi_\mathrm{a}^2\, e^{E_\mathrm{b}/(k_\mathrm{B}T)}$, with $\phi_\mathrm{d}(\phi_\mathrm{a})$ the dimer(atom) phase space density, respectively, as found in [5].

The results for this simple analytic model are shown in Fig. 4 of the main text as dashed black lines. Agreement is found for magnetic fields above 700 G. For lower magnetic fields the binding energy of the dimers is greater than $10\,\mu\mathrm{K}$ and the assumptions that all particles during three-body recombination and dissociation remain trapped is no longer valid.

Including Evaporation

For an accurate picture of the dimer formation, the evaporation ramp needs to be taken into account as our dimers are created during the last stage of evaporation. The evaporation ramp changes the rate equations because the rate coefficients now become time-dependent, as the temperature of the atom cloud changes with time. Furthermore, there is an additional loss channel for the atoms as they evaporate out of the trap. As atoms evaporate and the temperature of the cloud changes, the rate coefficients change according to, i.e. $R_{3r} \propto T_\mathrm{a}(t)$ and $C_d \propto [T_\mathrm{a}(t)]^{5/2}\, e^{-E_\mathrm{b}/(k_\mathrm{B}T_\mathrm{a}(t))}$, respectively.

During the evaporation ramp, the change in trapdepth U and atomnumber N, leads to a change in atom density which can be characterized by

$$\gamma(t) = \left[(1 - \frac{3}{2}\alpha)\frac{\dot{N}}{N(t)} + 3\frac{\dot{U}}{U(t)}\right] n_\mathrm{a}, \tag{8}$$

Here, α is the scaling parameter, whereby $T \propto N^\alpha$, and represents the temperature decrease per lost particle [8]. We assume an exponential evaporation ramp of duration τ_e. Thus $N(t) = N_\mathrm{i}\, e^{\left(\frac{t}{\tau_\mathrm{e}}\,\mathrm{Ln}\left[\frac{N_\mathrm{f}}{N_\mathrm{i}}\right]\right)}$ and $U(t) = U_\mathrm{i}\, e^{\left(\frac{t}{\tau_\mathrm{e}}\,\mathrm{Ln}\left[\frac{U_\mathrm{f}}{U_\mathrm{i}}\right]\right)}$, with $N_\mathrm{i}(N_\mathrm{f})$ the initial (final) atom number and $U_\mathrm{i}(U_\mathrm{f})$ the initial (final) trap depth at the beginning (end) of the evaporation ramp.

The full rate equations now become

$$\frac{dn_\mathrm{a}}{dt} = -4R_{3r}n_\mathrm{a}^3 + 4C_d n_\mathrm{d} n_\mathrm{a} - \gamma(t) \tag{9}$$

$$\frac{dn_\mathrm{d}}{dt} = 2R_{3r}n_\mathrm{a}^3 - 2C_d n_\mathrm{d} n_\mathrm{a}. \tag{10}$$

The results of solving these rate equations for our experimental parameters are shown as the blue line in Fig. 4 of the main text. Note that no free parameters are used and the experimental input parameters are obtained from time-of-flight (tof) data. See table I for the simulation input values and corresponding statistical uncertainities, as obtained from tof absorption

Parameter	Value
N_i	$17(3)\times10^4$
N_f	$33(2)\times10^3$
T_i (μK)	37(8)
α	1.1(2)
$n_\mathrm{a}^{(t=0)}$ (m^{-3})	$5(2)\times10^{16}$
U_i (μK)	73(54)
U_f (μK)	20(14)

TABLE I. Values of atom parameters used in the numerical solutions to the rate equations (solid lines, Fig. 4. main text) and based on time-of-flight (tof) absorption imaging. Errors come from the fit uncertainity of the parameters extracted from the tof fits.

images. The values for $N_\mathrm{i}, T_\mathrm{i}, n_\mathrm{a}(t=0), U_\mathrm{i}, U_\mathrm{f}$ and α are based on our evaporation ramp data, taken separately and rescaled to match the tof data of the ion-measurement day. For calculating the trap depth from the tof data, we use $U = \frac{\bar{w}_0^2}{4}\left(\sigma_\mathrm{x}^0\sigma_\mathrm{y}^0\sigma_\mathrm{z}^0\right)^{-2/3} k_\mathrm{B}T$, with average width $\bar{w}_0 = \left(w_\mathrm{x}\, w_\mathrm{y}\, w_\mathrm{z}\right)^{1/3} \approx (40\times40\times4000)\ \mu\mathrm{m} \approx 186\,\mu\mathrm{m}$ and $\sigma_\mathrm{z}^0 \approx 10\,\sigma_\mathrm{x}^0$. Here, σ_i^0 is the in-situ width of the cloud in the i-th direction with $i = (\mathrm{x},\mathrm{y},\mathrm{z})$. From the atom tof data we obtain both σ_x^0 and σ_y^0 and the trap ratio (1:10) gives the relation between σ_z^0 and σ_x^0. The final atomnumber N_f comes from the tof taken in between the ion-measurements on the same day. We check that the numerical simulation of the evaporation results in the final density and temperature as measured in these time-of-flights. The mean values for these datasets are $n_\mathrm{a} = 2.1(3)\times10^{16}\,\mathrm{m}^{-3}$ and $T = 5.6(2)\,\mu\mathrm{K}$.

Binding energy of the dimers

In the universal regime of the Feshbach resonance ($|a| \gg R_\mathrm{vdW}$), the binding energy is given by $E_\mathrm{b} = \hbar^2/(ma^2)$, with m the mass of the atom and R_vdW the van der Waals range. The scattering length a follows the general Feshbach relation [9, 10] of $a = a_\mathrm{bg} - \frac{a_\mathrm{bg}\Delta}{B-B_0}$. This shows that, by changing the magnetic field, we can tune the scattering length and change the binding energy of the dimers.

When calculating the binding energy for magnetic fields further away from the center, such that $a \gg R_\mathrm{vdW}$ does not hold, an additional correction to the universal expression of E_b needs to be taken into account, which comes from the non-zero range of the van der Waals potential [11]. Then

$$E_\mathrm{b} = \frac{\hbar^2}{m(a-\bar{a})^2}. \tag{11}$$

For the case of lithium $\bar{a} = 0.956R_\mathrm{vdW} = 0.956\times31.26a_0$ according to [3]. The dimers are created in the ${}^3\Sigma_u^+(\nu=-1)$ state, where ν is the vibrational quantum number counted down from the continuum [10]. This is the last molecular bound state of Li_2 which mixes with the entrance channel ($F = 1/2, m_\mathrm{F} = \pm1/2$) facilitating formation of Li_2 dimers.

Note that when we overlap the atoms with the ion, we ramp to zero-field to perform all experiments with the same dimer binding energy to avoid influences on the molecular ion formation rate [12] as well as quantum effects [13, 14]. For magnetic fields below 550 G the dimer bound state switches from ${}^3\Sigma_u^+(\nu=-1)$ to ${}^1\Sigma_g^+(\nu=-1)$ and with $S=0$ its magnetic moment vanishes. Consequently, the binding energy of the dimers becomes field independent and for zero-field they have a binding energy of about 1.38 GHz [10, 15].

Feshbach Resonance Parameters

The exact value of $E_\mathrm{b}(B)$ or $a(B)$ matters when we want to calculate the number of dimers we create. This value is closely related to the determination of the FR parameters of the FR we use to create the dimers. The most accurate and recent determination of the FR parameters stems from [16], where they measured the binding energy as a function of magnetic field directly and provide $a(B)$ for 0-2000 G. When doing a local fit ($|B-B_0| \ll \Delta$) to $a(B)$ using $a = a_\mathrm{bg} - \frac{a_\mathrm{bg}\Delta}{B-B_0}$, they found the fit parameters to be $a_\mathrm{bg} = -1582(1)\,a_0$, $B_0 = 832.18(8)\,G$, $\Delta = -262.3(3)\,G$. However this only applies for a narrow range of magnetic fields close to B_0. Farther away, a leading order correction term needs to be added because of another close-by FR at 527 G, as was shown in [17]. For our theory lines we therefore choose to directly take $a(B)$ as given by [16] and use Eq. 11 to calculate the binding energy.

Tuning the dimer density

To explore different Li_2 densities in our system, we either tune P_ODT or B_{Li_2} at the final stage of the evaporative cooling in the experimental sequence, as it is depicted in Fig. 2. We tune the atoms' phase space density, by changing the ODT depth at the end of evaporation with the help of an acousto-optical modulator. This changes both the density of the atoms as well as their temperature. The P_ODT is the power of the optical dipole beam when entering the setup. This beams creates the crossed dipole trap by entering through the endcaps of the ion trap at an angle of 5° with respect to the Paul trap axis as depicted in Fig.1 of the main text. Using a lin $\perp$ lin polarization configuration, we prevent the occurrence of an optical lattice potential.

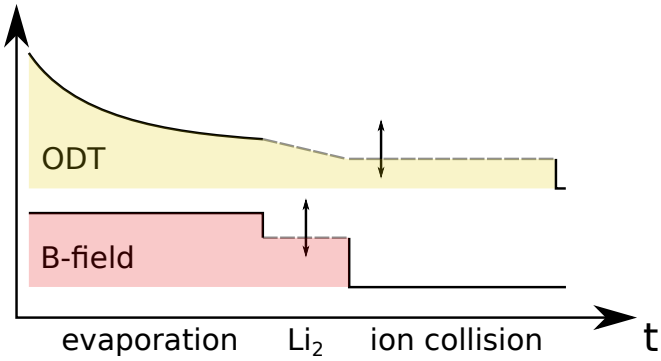

FIG. 2. Sketch of evaporation sequence to tune the dimer density in Li-Li_2 mixture before overlap with a single ion. We either vary the magnetic field or the trap depth of the final evaporation stage.

When changing the magnetic field to $B_{\mathrm{Li}_2} = 600 - 760\,\mathrm{G}$, we found that the atom density stays constant as the amount of dimers created stays below the experimental error (about 20) for determining the atom density. This is further confirmed by the constant charge exchange rate measured by the ion and from independent time-of-flight measurements. When changing B_{Li_2}, the scattering length changes and thus the dimer binding energy. This leads to a variable dimer density as the recombination rate and dissociation rate are depending on E_{b}.

ATOM DATA FOR P_{ODT} SCAN

We take regular time-of-flight measurements of the atomic cloud using absorption imaging after we transport the ODT to the center of the Paul trap. We typically average 4-5 images before fitting a Gaussian distribution to extract the atom parameters, i.e. atom number and width of the cloud. The coldest atom clouds have a temperature as low as $0.9(5)\,\mu$K with about 5×10^3 atoms. However the presence of the ion trap limits the numerical apperture of our imaging system and the coldest clouds are only a few pixels wide and when expanding become quickly to dilute too detect.

From the time-of-flight curves, assuming free expansion, the atomnumber N_{a}, temperature T_x and T_y as well as the in-situ width of the cloud, σ_x^0 and σ_y^0, in both x- and y- direction can be obtained. This follows from fitting the expansion of the width of the cloud as a function of expansion time using

$$\sigma_i(t) = \sqrt{(\sigma_i^0)^2 + \frac{k_B T}{m_a}\, t^2} \tag{12}$$

whereby the in-situ width of the cloud is related to the trapfrequency by $\sigma_i^0 = \left(\frac{kT}{m\omega_i^2}\right)^{1/2}$, with trap frequencies

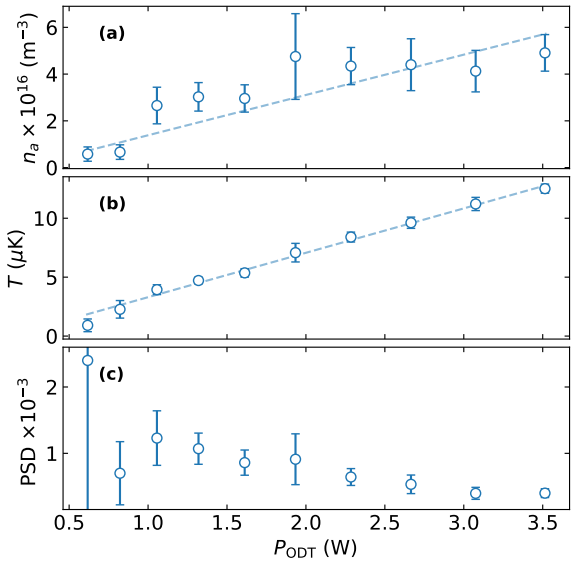

FIG. 3. Atom parameters for optical dipole trap power scan. The atom density a), temperature b) and phase space density (PSD) c) are obtained from time-of-flight absorption imaging measurements. The dashed lines are linear fits and guides for the eye. The atom PSD in c) is related to the increase in dimer phase space density. Here, the error bars reflect the total statistical uncertainties. Note the high error bars for the lowest point ($P_{\mathrm{ODT}} \approx 0.7\,\mathrm{W}$) in c), showing the limitations of our imaging method.

ω_i and $i = (\mathrm{x}, \mathrm{y}, \mathrm{z})$.

The peak density n_{a} for a thermal cloud in an harmonic trap is given by

$$n_{\mathrm{a}} = \left(\frac{\bar{\omega}^2\, m_{\mathrm{a}}}{2\pi\, k_{\mathrm{B}}\, T_a}\right)^{3/2} N = \frac{N}{(2\pi)^{3/2}\sigma_{\mathrm{x}}^0\, \sigma_{\mathrm{y}}^0\, \sigma_{\mathrm{z}}^0} \tag{13}$$

Here, $\bar{\omega}^2$ is the geometrical average of the trap frequency and it can be calculated as $\bar{\omega}_i = (\omega_{\mathrm{x}}\omega_{\mathrm{y}}\omega_{\mathrm{z}})^{1/3}$. Furthermore $T = (T_{\mathrm{x}} + T_{\mathrm{y}})/2$ and $\sigma_{\mathrm{z}}^0 = 10\,\sigma_{\mathrm{x}}^0$ for our trap. The phase space density is given by

$$\phi_{\mathrm{a}} = n_{\mathrm{a}}\, \lambda_{\mathrm{dB}}^3 = n_{\mathrm{a}} \left(\frac{2\pi\hbar^2}{m_{\mathrm{a}} k_{\mathrm{B}} T_{\mathrm{a}}}\right)^{3/2}. \tag{14}$$

For the P_{ODT} scan, the observed atom density n_{a}, temperature T and phase space density ϕ_{a} are shown in Fig. 3.

We can model the dimer density using the thermal equilibrium model (Eq. 7) based on the atom data corresponding to Fig. 2b (main text), which only requires the final atom number and temperature as input. This model is shown in Fig. 4 (black dashed line) with a 20% error range in atom temperature (black dotted lines). The model confirms the trend we see in the ion-measurements.

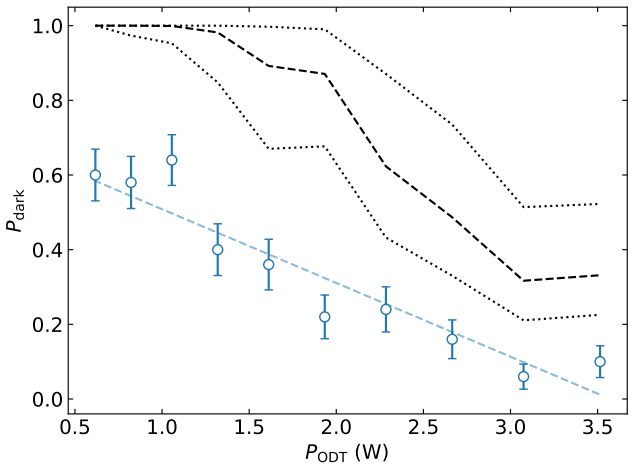

FIG. 4. Dark Yb^+ ion probability as a function of the ODT power. The experimental data (blue disks) is the same as in Fig 2 a) of the main text and the black lines are the solution of Eq. 7 for the given experimental parameters and assuming thermal equilibrium. The black dotted lines account for a 20% error in the atom temperature, typical for time-of-flight measurements.

Furthermore, the overestimation of the dark ion probability is similar to the result in Fig. 4a (main text), where the ion-measurement at 693 G is also overestimated by the black curve. Further benchmarking of the evaporation ramps used in this dataset would allow us to include the evaporation ramp and numerically model the dimer density. This requires additional measurements of the initial atom number, temperature and density at the start of the evaporation ramp, as well as the initial trapdepth. Furthermore, for each datapoint we varied the final trapdepth and this affects the scaling parameter α that describes the evaporation and this would have to be individually benchmarked as well. Nevertheless the simple thermal equilibrium model can qualitatively explain the observed increase in the probability of the molecular ion formation for lower P_{odt} as observed in the main text (Fig. 2).

[1] D. Leibfried, R. Blatt, C. Monroe, and D. Wineland, Rev. Mod. Phys. **75**, 281 (2003).
[2] A. Mohammadi, A. Krükow, A. Mahdian, M. Deiß, J. Pérez-Ríos, H. da Silva, M. Raoult, O. Dulieu, and J. H. Denschlag, Phys. Rev. Research **3**, 013196 (2021).
[3] R. Grimm, "Ultracold Fermi gases in the BEC-BCS crossover: a review from the Innsbruck perspective," in *Ultra-cold Fermi Gases*, edited by M. Inguscio, W. Ketterle, and C. Salomon (2008) Proceedings of the International School of Physics "Enrico Fermi", Course CLXIV, Varenna, 20-30 June 2006.
[4] W. Zwerger, ed., *The BCS-BEC Crossover and the Unitary Fermi Gas*, Lecture Notes in Physics, Vol. 836 (Springer, Berlin Heidelberg, 2012).
[5] C. Chin and R. Grimm, Phys. Rev. A **69**, 033612 (2004).
[6] S. J. J. M. F. Kokkelmans, G. V. Shlyapnikov, and C. Salomon, Phys. Rev. A **69**, 031602(R) (2004).
[7] D. S. Petrov, Phys. Rev. A **67**, 010703 (2003).
[8] W. Ketterle and N. J. van Druten, Adv. At. Mol. Opt. Phys. **37**, 181 (1996).
[9] A. J. Moerdijk, B. J. Verhaar, and A. Axelsson, Phys. Rev. A **51**, 4852 (1995).
[10] C. Chin, R. Grimm, P. Julienne, and E. Tiesinga, Rev. Mod. Phys. **82**, 1225 (2010).
[11] G. F. Gribakin and V. V. Flambaum, Phys. Rev. A **48**, 546 (1993).
[12] H. Hirzler, E. Trimby, R. S. Lous, G. C. Groenenboom, R. Gerritsma, and J. Pérez-Ríos, Phys. Rev. Research **2**, 033232 (2020).
[13] M. Tomza, K. Jachymski, R. Gerritsma, A. Negretti, T. Calarco, Z. Idziaszek, and P. S. Julienne, Rev. Mod. Phys. **91**, 035001 (2019).
[14] P. Weckesser, F. Thielemann, D. Wiater, A. Wojciechowska, L. Karpa, K. Jachymski, M. Tomza, T. Walker, and T. Schätz, arxiv:2105.09382 (2021).
[15] P. S. Julienne and J. M. Hutson, Phys. Rev. A **89** (2014).
[16] G. Zürn, T. Lompe, A. N. Wenz, S. Jochim, P. S. Julienne, and J. M. Hutson, Phys. Rev. Lett. **110**, 135301 (2013).
[17] M. Bartenstein, A. Altmeyer, S. Riedl, R. Geursen, S. Jochim, C. Chin, J. H. Denschlag, R. Grimm, A. Simoni, E. Tiesinga, C. J. Williams, and P. S. Julienne, Phys. Rev. Lett. **94**, 103201 (2005).